Article

Using Climate-Sensitive 3D City Modeling to Analyze Outdoor Thermal Comfort in Urban Areas

SeyedehRabeeh HosseiniHaghighi [1,†], **Fatemeh Izadi** [1,†], **Rushikesh Padsala** [2,†]
and Ursula Eicker [1,*]

1   Department of Building, Civil, and Environmental Engineering, Concordia University,
    Montréal, QC H3G1M8, Canada; seyedehrabeeh.hosseinihaghighi@mail.concordia.ca (S.H.);
    fatemeh.izadi@mail.concordia.ca (F.I.)
2   Faculty of Geomatics, Computer science, and Mathematics, Hochschule für Technik Stuttgart,
    Schellingstr. 24, 70174 Stuttgart, Germany; rushikesh.padsala@hft-stuttgart.de
*   Correspondence: ursula.eicker@concordia.ca
†   These authors contributed equally to this work.

Abstract: With increasing urbanization, climate change poses an unprecedented threat, and climate-sensitive urban management is highly demanded. Mitigating climate change undoubtedly requires smarter urban design tools and techniques than ever before. With the continuous evolution of geospatial technologies and an added benefit of analyzing and virtually visualizing our world in three dimensions, the focus is now shifting from a traditional 2D to a more complicated 3D spatial design and assessment with increasing potential of supporting climate-responsive urban decisions. This paper focuses on using 3D city models to calculate the mean radiant temperature (Tmrt) as an outdoor thermal comfort indicator in terms of assessing the spatiotemporal distribution of heat stress on the district scale. The analysis is done to evaluate planning scenarios for a district transformation in Montreal/Canada. The research identifies a systematic workflow to assess and upgrade the outdoor thermal comfort using the contribution of ArcGIS CityEngine for 3D city modeling and the open-source model of solar longwave environmental irradiance geometry (SOLWEIG) as the climate assessment model. A statistically downscaled weather profile for the warmest year predicted before 2050 (2047) is used for climate data. The outcome shows the workflow capacity for the structured recognition of area under heat stress alongside supporting the efficient intervention, the tree placement as a passive strategy of heat mitigation. The adaptability of workflow with the various urban scale makes it an effective response to the technical challenges of urban designers for decision-making and action planning. However, the discovered technical issues in data conversion and wall surface albedo processing call for the climate assessment model improvement as future demand.

Keywords: 3D city models; spatial design; outdoor thermal comfort; mean radiant temperature

1. Introduction

Canada's Changing Climate Report has announced a doubled rate of warming for Canada compared to the rest of the world [1]. The Crowther Lab at ETH Zurich University has predicted that some Canadian cities will experience an average temperature increased by more than three degrees Celsius by 2050. It is estimated at 3.1 °C for Montreal [2]. Figure 1 shows the predicted increase of stress days across Canadian cities for the projected years starting in 1961. The impact of heat stress is already being felt by increasing the number of hot days, more than 30 °C [3]. The rising frequency of heatwaves in many Canadian cities resulted in the death of 70 people in 2018 in Quebec alone [4]. Health Canada (2011) reported that when the daily average temperature goes higher than 20 °C in

seven Canadian cities, the relative mortality rate rises by 2.3% for every degree increase. This means the intensity of 2–3 °C would lead to a 4–7% increase in the mortality rate [5]. Environment Canada (Ontario Region) introduces the heatwave as a period in which, for three successive days, the maximum temperatures stay or go over 32 °C [6]. However, the air temperature is not the only factor for heat. The daily thermal experience is quite complex; for the same day and air temperature, there is a different feeling on a different pathway.
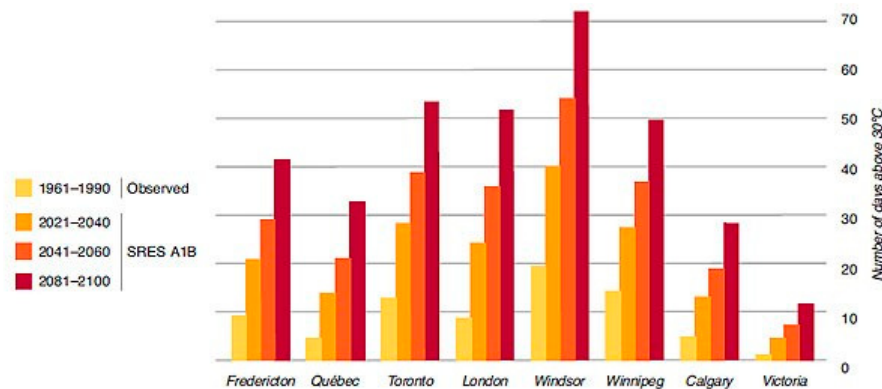

Figure 1. Current and projected number of days exceeding 30 °C for Canadian cities [3] based on the observed temperature data between 1961 and 1990.

Human thermal comfort in the urban space is associated with four environmental parameters: air temperature, relative humidity, air velocity, and thermal radiation, which is the most complicated parameter. The thermal radiation within an urban open space is usually described by mean radiant temperature (Tmrt), which is defined as a precise measurement of urban sites prone to heat [7]. Thorsson et al. (2014) identified it as a better indicator of the harmful heat stress condition [8]. Tmrt depends on the temperature difference and the radiant net exchange between the object and the surrounded environment [9]. Thus, the potential of a surface to absorb or negate heat and the amount of object seen by surrounding radiation sources has a crucial influence on Tmrt variation. The local convection coefficient is another practical factor for increasing Tmrt in the dormant area. If the wind speed decreases, the portion of radiation in the global temperature increases; in turn, Tmrt grows more [10].

In the urban area, the physical characteristics of the built environment affect the distribution of Tmrt by changing the exposure to sunlight and the material coverage of the surfaces. When the intra-urban temperature shows a slight variation during the day, the Tmrt represents a considerable variation over short distances resulting in a noticeable difference in thermal perception [11,12]. The effect of urban form on thermal comfort focused on the Tmrt indicator has been the subject of much research for different climate zones using simulation method or real data observation analysis [11–15]. Two principle geometry factors in evaluating the heat stress of urban spaces include the aspect ratio, the ratio of building height to the street width and, sky view factor, representing the surface exposure to the skydome, ranging from zero to one [12–14]. The finding highlighted the open structure design with low-rise buildings, and the lower aspect ratio is prone to increase the number of extreme heat stress hours. In contrast, the street canyon with a smaller sky view factor, shaded by surrounding buildings, provides more comfortable with lower Tmrt during summer days [12,15,16]. For canyons of the same aspect ratio, their orientation has an influential role in managing the Tmrt [13]. However, it is recommended to consider the simultaneous impacts of all critical factors such as the aspect ratio, canyon orientation, level of urban density and, latitude of canyon location [12,13,16,17].

The management of geometry parameters is costing financially and needs to be considered in the first place since they will not change over a long period of time. Although a dense structure maintains the extreme swings in Tmrt and daytime thermal stress during seasons [12,13], without respecting the flexible mitigators such as vegetations or adequate ventilation, it could increase nighttime temperature

due to the urban heat island effects during summer [12]. The contribution of urban heat island on the local scale and the increase of temperature at the regional level intensify the heat stress in the outdoor spaces [12,18]. Many studies showed the potential of Tmrt reduction through urban vegetation [11,14–16,19]. Planting trees is an effective measure to improve the urban microclimate by reducing summer day temperature within the tree's boundaries and beyond the leeward side [19–21]. In addition to their ecological, aesthetic, health and, physiological benefits, the distribution and density of trees also allow flexible strategies to manage sun exposure in urban areas. Trees help reduce the transmission of solar radiation [15,16] and enhance the evapotranspiration and improve the shading pattern on surfaces underlying heat stress conditions [21]. A more extensive canopy means a more significant contribution in reducing temperature and decreasing Tmrt in both daytime and nighttime. The effect of clustered tree planting is more than the isolated placement of trees in Tmrt reduction at low density and low height structure [15,19]. However, dense construction must prioritize tree placement in areas not currently shaded by other sources like buildings, particularly in areas with heavy pedestrian traffic [14,15].

The effect of surrounded coverage is another concern of designers to manage Tmrt through the albedo of surface materials. Albedo is a physical property of the material to change the thermal behavior of the surrounded environment. Albedo refers to the fraction of solar radiation reflected by a projected surface [22]. Materials with low albedo, dark-colored, tend to absorb radiation and contribute to the urban heat island, while surfaces with a high albedo, white-colored, are prone to reflect it. Although using high albedo material is recommended for buildings to save energy during summer time [20], it is a less desirable solution on the surfaces near the ground where the reflected beams bounce back to urban spaces where human activities are present [23]. Alchapar, E.N. Correa (2015) demonstrated albedo's effect on the temperature variation of surrounded surfaces, particularly in the high-density area, higher aspect ratio and, larger wall surfaces. When albedo increases by 10%, the air temperature increases by 0.5 K to 0.7 K, whereas it does not significantly change the low-density area [24]. It is essential to highlight that the impact of albedo is not constant during the day. Hui Li (2016) examined that the effect of albedo is at the highest level during the early morning and late afternoon. While during midday, it tends to a low and constant value, and cloudy days intensify it as well [25]. The summation of shortwave and longwave fluxes outgoing from the surrounded surfaces is comparatively small to incoming fluxes originating from the cardinal points [14,23]. Hence, the simulated albedo effect is expected to be small, given the different turbulence evened out in local air temperature.

The complexity of outdoor thermal conditions in response to Tmrt, as a significant indicator of thermal comfort, demands the combination of 3D city modeling and climate assessment program to support climate sensitive spatial design. Traditional urban design methods were mostly based on 2D spatial design. However, with the continuous evolution of geospatial technologies and the added benefit of analyzing and virtually visualizing our world in three dimensions, it is possible to model and evaluate the reflection of the urban decisions before implementation and reduce the cost of trial errors. Thus, this research aims first to make use of 3D city modeling tools to design and create the study area and then uses these 3D city models to calculate the mean radiant temperature (Tmrt) in terms of assessing the spatiotemporal distribution of the heat stress for an upcoming transformed district in the city of Montreal. Alongside that, the study introduces a systematic workflow to evaluate and improve outdoor thermal comfort through the accurate placement of vegetation (trees), convenient in city scale.

2. Materials and Methods

2.1. Study Area and Scenario Development

Montreal is situated (45.50° N and 73.56° W) at the conflux of several climatic regions and is classified as humid continental [26]. The coldest month of the year is January, with a daily average temperature of −9.7 °C, although due to the wind chill, the feeling temperature decreases more than the actual temperature. The warm months start from mid-May to mid-September, with an average

daily temperature of 20 °C. The hottest month is July, with an average daily high of 26.3 °C and lower nighttime temperatures of 21.2 °C. High humidity resulting from surrounded waterbodies turns the feeling temperature to higher than the summer's actual temperature, and some nights temperature remains at an uncomfortable degree. The clear days last for 4.5 months, beginning in June and ending in October. Almost 64% of the year, Montreal's sky is clear, mostly clear or partly cloudy. During the bright days, an average daily incident shortwave energy per square meter goes above 5.6 kWh and reaches 6.7 kWh on June 30. Variation of wind for cold days versus warm days is less than 1 m/s, and during calm and warm days of summer, the average speed is almost 4 m/s from the south direction.

The study area, Dominion Bridge within the borough of Lachine East, is a low-rise industrial site lying on land with a 3 m difference between north and south of the site that covers around 10 ha, located in the south of Montreal island. The area is surrounded by residential land uses planned for mid to high-rise development from north, south, and east, while the west side is fully developed with low-rise residential buildings, see Figure 2. The developers are interested in turning Dominion Bridge into a dense and high-rise area with residential buildings. The municipality and its mayor firmly intend to develop an eco-quartier with a resilient design, low levels of building energy consumption, using onsite energy generation, and improving human thermal comfort in outdoor urban spaces. Regarding the district's zoning bylaw, the floor area ratio equals 3, and the lot coverage ratio equals 40%. The site provides an above 250,000 sqm floor area distributed in the different building configuration layout and height. Since the site carries valuable history and heritage and tends to accommodate more than 2700 households, the combination of community and urban spaces were designed to serve different purposes and activities in the site.
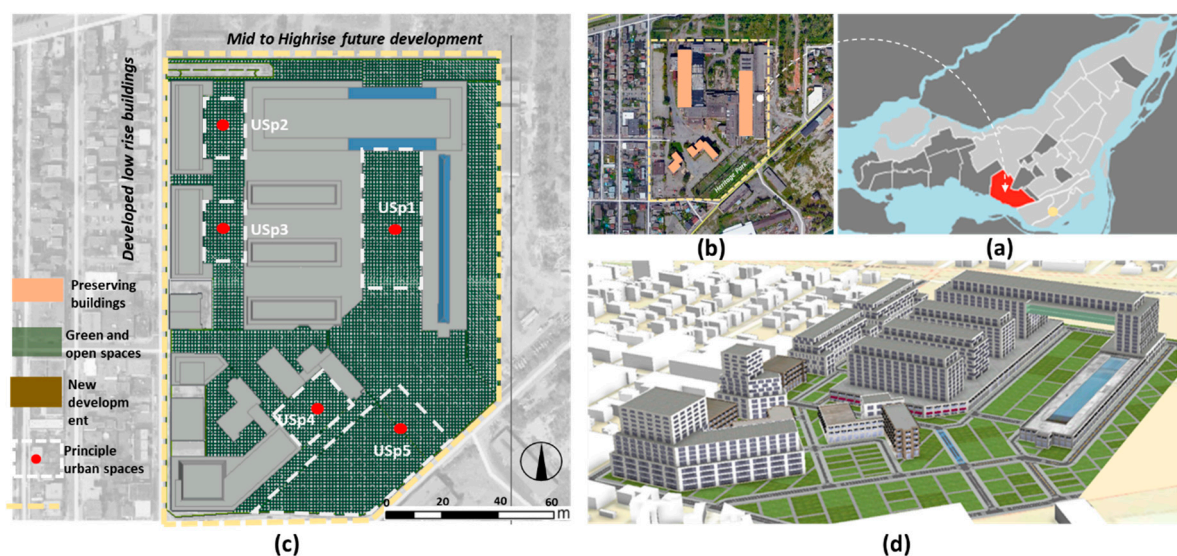

Figure 2. Location and spatial design and distribution of urban spaces in the study area: (**a**) Study area location in Lachine neighborhood on Montreal Island; (**b**) patrimonial building preserved in the study area; (**c**) the alternative master plan and focal urban spaces within the study area; (**d**) bird view of buildings bulk distribution and pathways connecting urban spaces and buildings generated through ArcGIS CityEngine.

Based on the above sets of boundary conditions and local zoning bylaws, 3D city models, including buildings, street networks, landscape, and trees, were modeled using ArcGIS CityEngine. CityEngine is part of ESRI software suites enabled for interoperability with GIS software such as ArcGIS Pro [27] and partially with the open-source software QGIS. Whereas the traditional and manual 3D modeling software such as SketchUp, Rhinoceros3D, or Autodesk 3D software, CityEngine can generate 3D city models leveraging its underlying shape grammar technique to program procedures and set parameters to generate and iterate large-scale 3D city models in considerably less amount

of time. Such a parametric procedural modeling technique using shape grammar offers a powerful 3D city modeling and visualization toolset, allowing quick visualization of complex city models, scenario development, and iterative urban design workflows [28]. Additional integration of a 3D vegetation library and inbuilt support to 3D objects for street furniture helps to make ArcGIS CityEngine a specialized 3D city modeling tool. For data conversion to other data formats, software such as feature manipulation engine (FME) provides a complete read and write support to CityEngine. The CityEngine derived 3D city models can be converted to various other 3D data formats such as COLLADA, gITF, FBX, OBJ, 3D multipatch shapefile, and file geodatabase (FGDB). Additionally, using FME, 3D city models from CityEngine can also be converted to the Open Geospatial Consortium (OGC) standardized open data model of CityGML in its different levels of details [29].

Although CityEngine is not open-source software, its application in the present work is highly motivated by its adaptability by city designers [30] as a specialized "3D urban modeling software" and creating all 3D city model elements. One such software is "Random3Dcity" [31]. Random3Dcity is an open-source procedural 3D city modeling software. However, due to its certain limitations, such as first, it is an experimental engine developed only as a prototype to be a first of its kind open-source procedural 3D city modeling tool. The second, its main priority is to procedurally generate 3D building geometries, giving the other elements of 3D city models such as vegetation, landcover, streets, and street furniture. That means the least amount of support and functionality. Thus, for the present work, the use of Random3Dcity was deemed not suitable. Another commercially available alternative is Rhinoceros3D [32], a computer-aided design (CAD) software widely used by city designers worldwide. Rhinoceros3D, when plugged in with Grasshopper, makes the 3D modeling parametric. The combination of Rhinoceros3D with Grasshopper and many different available plugins makes it a design environment that facilitates designing and analysis, all under one workspace. However, for analysis in the present work, QGIS plugin SOLWEIG needs to be used. Due to various technical shortcomings such as lack of direct support to coordinate systems, data interoperability issues with GIS software, no inbuilt and direct support to model other elements of 3D city models such as streets, landcover, and vegetation, Rhinoceros3D was also neglected.

The proposed design provides an urban scenario with a combination of urban spaces (USp) and walking pathways in the various spatial scales and orientation, see Figure 2. Following the designed function and active timing for each urban space, they are divided into four categories, the urban space with the intention of public gathering (USp_1), the local community spaces (USp_2–USp_4), and the public-heritage park as an accessible space for public use (USp_5). The final group of spaces as the medium spaces (USp_medium) located between principal urban spaces (USp_1 to USp_5) and connected them to buildings is divided into two groups according to the measurement of sky view factor, below 0.45 and above 0.45. From the energy-efficient design perspective for building construction, different setbacks have been considered from the street line to prevent the mutual shading of buildings and increase the efficient solar access in terms of heating demand reduction. This strategy has shaped wide canyons with a non-uniform and detached urban edge at 15 m above the street line, which affects the sky view factor of urban spaces unequally and results in the variation of shadow pattern on the ground.

Regarding the study area's complicated geometry in three dimensions, the 2D measurement of aspect ratio is not reliable and does not reflect the openness of urban spaces to the sky. While each point's sky view factor in the outdoor spaces clearly demonstrates the quality of sun exposure and radiation accessibility for that spot. The average sky view factor of points fall into each urban space is measured through the mean radiant temperature simulation process and listed in Table 1.

Table 1. Characteristics of principle urban spaces.

Urban Parameters	USp_1	USp_2	USp_3	USp_4	USp_5
Avg. Sky view factor	0.70	0.56	0.56	0.71	0.97
Orientation	N_S	N_S	N_S	NE_SW	Open
Activity purpose	Public square	Community purposes_private		Community purposes_public	Public Park

2.2. Spatial Modeling and Simulation of Mean Radiant Temperature (Tmrt)

Following the aim of research for ameliorating dense building construction concerning the outdoor thermal condition and retrieving the effect of regional temperature increment for a time ahead, we leveraged a procedure using two modeling tools: SOLWEIG as a climate assessment model for measuring the mean radiant temperature (Tmrt) in complicated urban geometry, and ArcGIS CityEngine as a spatial modeling tool to generate and convert 3D city models to adopt the format required by SOLWEIG consisting of the digital elevation model (DEM) and the digital surface model (DSM). DEM also is known as the bare earth model or also the digital terrain model (DTM), the digital representation of elevation data depicting real-world terrain profiles. A DSM is a digital surface model that, in addition to DEM, also represents elevation data of physical objects present on top of the terrain, such as buildings, streets, and landcover. The workflow presented in Figure 3 intends to evaluate the spatial distribution of the mean radiant temperature in the outdoor area resulting from building layout. The output helps discover the effect of building geometry in the distribution of shadow and sunlit area translated to the Tmrt map. Comparing the result with the physiological equivalent temperature (PET) index allows clustering areas above the threshold and prepare the hot-spots map representing the zones with a higher demand for heat mitigation practices. This stage's outcome will be used as the input for the remodeling process within CityEngine and applying systematic tree generation process as a response action to the efficient heat reduction.
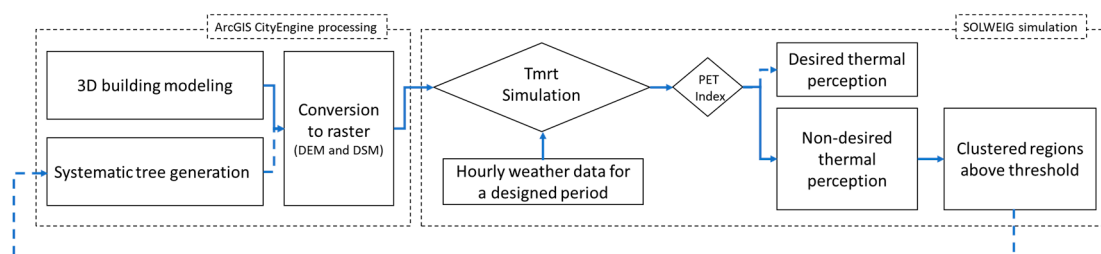

Figure 3. The flowchart of outdoor thermal assessment and improvement via systematic tree generation as the passive heat mitigation strategy.

2.3. 3D City Modeling

To better produce and manage 3D city models, ESRI has developed the 3D City Information Model (3DCIM). CityEngine, the 3D city modeling tool used in the present work, allows us to model the 3DCIM thematic structure shown in Figure 4. The use of the 3DCIM thematic structure also satisfies the data inputs required to run the SOLWEIG model. Although SOLWEIG does not take 3D city models as a direct input for its execution, DEMs and DSMs can be easily derived from the 3D city models using ESRI's ArcGIS Pro or FME.
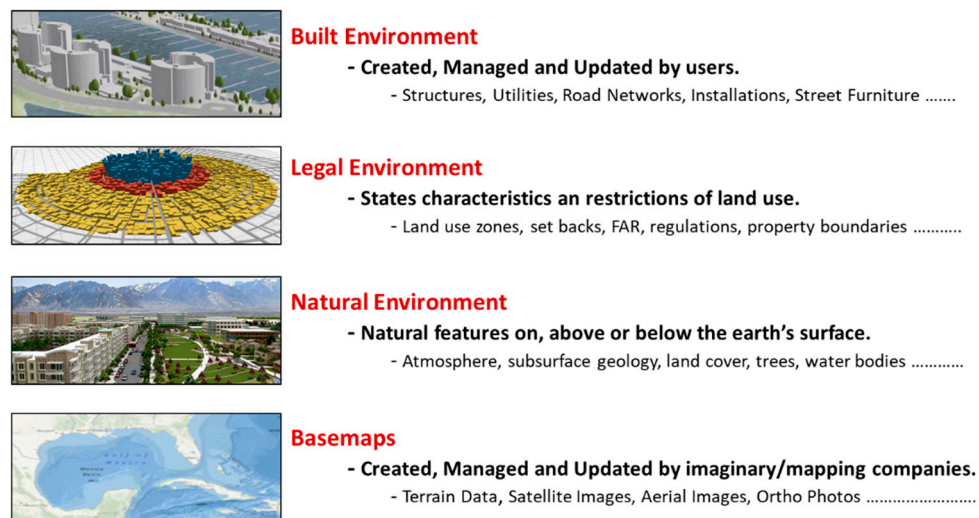
Figure 4. The 3D City Information Model (3DCIM) thematic structure by ESRI [33].

The present work, the district of Dominion Bridge in Montreal, is modeled based on the 3DCIM thematic structure using CityEngine. First, the terrain data (base map) is extracted and converted to a geotagged image file format (GeoTiff) from the available CityGML terrain (TINRelief) data of Montreal [34]. Further, taking the extracted terrain data as the elevation source, 3D city models in terms of buildings, pathways (built environment) and land cover, trees (natural environment) were modeled according to the mentioned zoning using the CGA rule file in ArcGIS CityEngine. For modeling buildings, the CityEngine inbuilt CGA shape grammar rule file named "Generic Modern Buildings.cga" was used and tweaked to fit the study area's zoning bylaws and boundary conditions, as explained in Section 2.1, see Figure 5a. For modeling landcover and its internal pathways, a publicly available CGA shape grammar rule file for landscape design named "greenspace construction.cga" was tweaked and used; see Figure 5b. Then, for modeling, structural pathways, and connected sidewalks, an updated version of the publicly available ESRI's complete street CGA shape grammar rule file published by D. Wasserman (2020) [35] was tweaked to fit the boundary conditions of the study area, see Figure 5c. Since the first purpose of the presented work is to use 3D city models to mitigate the heat stress of urban space during heat days of summer, 3D vegetation objects were placed based on the urban heat stress hotspot map produced by the SOLWEIG model. Commonly found deciduous tree species in Montreal's city from the maple tree family "Norway maple (*Acer platanoides*)" is used as it suits our intention to investigate the shadow pattern in the urban and open spaces [19]. A realistic representation of Norway maple available in the ESRI 3D vegetation library [35] is used to symbolize trees in CityEngine. Since the proposed design was focused on being used as an input to SOLWEIG, buildings were modeled in the level of detail (LoD) 2, and landscape, trees, and pathways were modeled in LoD 3, see Figure 5d.

As an input to the SOLWEIG model, all the above 3D city models were rasterized using ArcGIS Pro. For data consistency and to satisfy the SOLWEIG model's prerequisite, all the raster data were produced with the same spatial resolution (1 m) and coordinate system NAD_1983_CSRS_MTM_8. This coordinate system is chosen because Montreal's available open data are also modeled with the same coordinate system. The output from the conversion of CityEngine 3D city modeling consists of the DEM representing the terrain, DSM representing buildings with terrain, landcover representing the distribution of pathways, buildings, and the landscape for the study area, and canopy digital surface model (CDSM) representing trees.
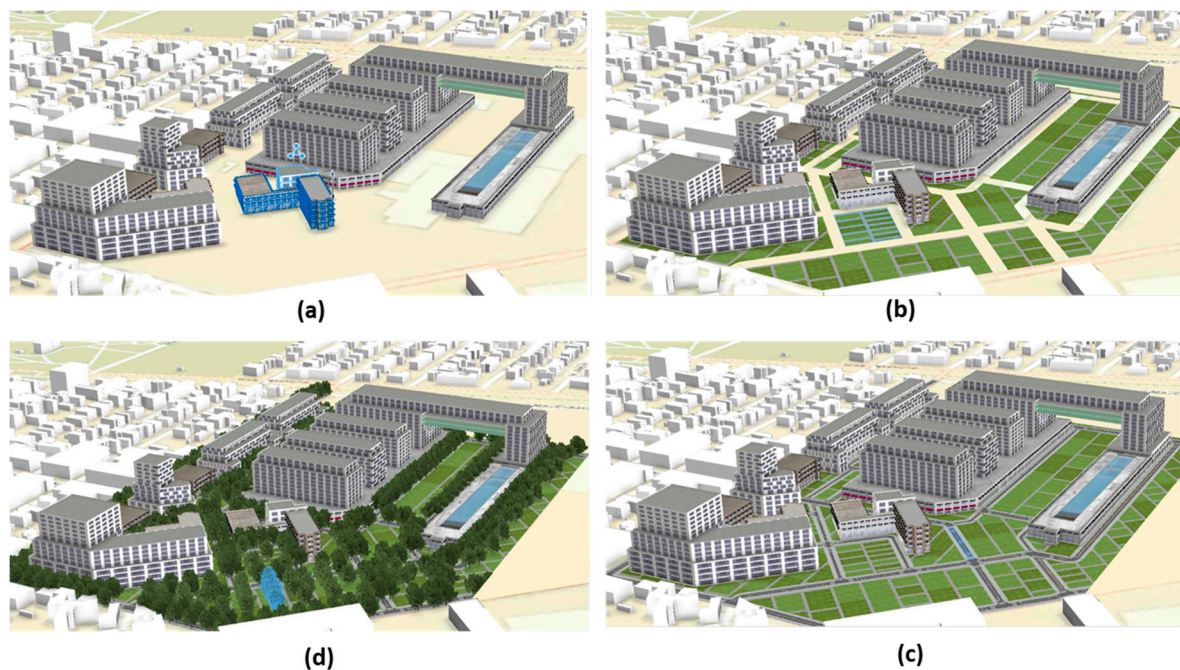
Figure 5. The process of Dominion Bridge modeling through ArcGIS CityEngine: (**a**) The textured 3D building modeling; (**b**) the landcover modeling (landscape + internal pathways): (**c**) the pathway modeling: (**d**) the realistic (LoD3) 3D tree modeling using the 3D Norway maple tree model in ArcGIS CityEngine.

However, the above-modeled buildings' rasterization, particularly one 3D building geometry, as shown in Figure 6, faced a technical constraint. The output DSM generated using 3D building geometry, and its underlying terrain resulted in interpolated elevation values instead of preserving its no data cell values for the open space between the horizontal bridge building and the terrain surface.
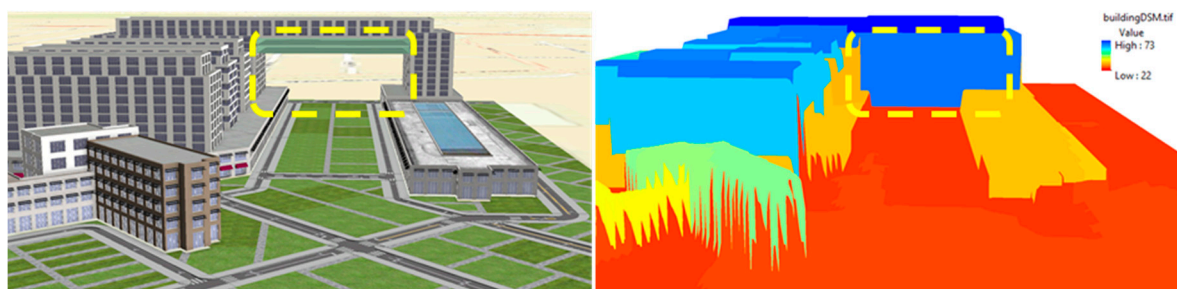

Figure 6. Open space as a part of 3D building geometry interpolated with elevation cell values in its DSM.

One possible explanation for such an error in the DSM can be that since the building DSM is a summation of the building and terrain elevation cell values, the open space below the horizontal bridge-building is also by default considered a part of the building. The elevation cell values are interpolated based on the elevation cell values of the underlying terrain and the bottom surface of the horizontal bridge-building. Such complications lead to an incorrect analysis for building geometries such as in Figure 6 in simulation models such as SOLWEIG for which primary inputs are raster datasets. For a proper analysis of these complex building geometries that are easy to find in the real world, the SOLWEIG model and other similar models need to be further developed to directly take 3D city models as input instead of converting them into a DSM, which leads to a loss of data/information.

2.4. SOLWEIG Simulation Model

The spatial variations of Tmrt are calculated using the SOLWEIG model. SOLWEIG is the open-source model of SOlar Long Wave Environmental Irradiance Geometry, a climate design program assembled on Urban Multi-scale Environmental Predictor (UMEP). UMEP is an extendable plugin for the QGIS, open-source desktop geographic information systems (GIS) that enables spatial data visualization and analysis capabilities [36]. SOLWEIG is suitable for analyzing the complex interaction of urban geometry and thermal environment at a district scale when the extended meteorological datasets are available [37]. It is a validated model to measure Tmrt resulted from the complex geometry of the built environment using 3D short and longwave radiation flux [11,14,15,37–40]. Comparing SOLWEIG with other parallel models (ENVI-met and Ray Man), Gála and Kántor (2020) demonstrated that the SOLWEIG model is highly reliable to predict the daytime Tmrt during the hottest period of the day, around noon and afternoon, when the local air temperature reaches the peak. However, for points located near the physical obstruction (e.g., close to buildings), using the domain-wide mean surface temperature leads to an overestimation of Tmrt where the site is in the shade and an underestimation where the site is sunlit. Moreover, when the sun elevation decreases, the rate of expectation for Tmrt errors increases as well [40].

SOLWEIG derives Tmrt from the Stefan–Boltzmann law using the mean radiant flux density, which is the result from the summation of all long and shortwave radiation fields in three dimensions on a standing person at the level of 1.1 m, where the angular factor is set to 0.22 for radiation fluxes from four lateral cardinal points and 0.06 for radiation fluxes from above and below sides [11,37]. It is noted to highlight the reflected fluxes are equally shared between the cardinal points [37,38], so, for the nonuniformed sky-obstructions (e.g., next to buildings), the model tends to errors in reflected fluxes [39]. The model assumes 0.7 and 0.97 for the absorption coefficients of short wave and longwave radiation, respectively. The default value of albedo is 0.20, and the emissivity of buildings and vegetation is considered 0.95. There is an empirical relationship between environment surfaces and air temperature where the sky is clear. The proportion of received sun stream for each surface depends on the anisotropic sky view factor and sun altitude [37]. Wind velocity is not included in the model. However, a future aim is to couple with a surface energy model and a convective boundary model to add the possibility of physiological equivalent temperature (PET) calculation [36]. In terms of satisfying the input datasets for SOLWEIG modeling, two datasets are required in various formats, meteorological data, and spatial data. The meteorological data sets for an alternative temporal period consist of air temperature ($°C$), specific humidity ($kg.kg^{-1}$), barometric pressure (Kpa), wind speed ($m.s^{-1}$), relative humidity (%), hourly incoming shortwave radiation ($W.m^{-2}$) and rainfall rate ($kg.m^{-2}. s^{-1}$) as obligatory parameters which are explained in the next section.

The spatial dataset is provided as the urban scenario and converted to DEM and DSM format at the district level. Using spatial data in the SOLWEIG model needs to pass the preprocessing level. In this case, building DSM and ground DEM are processed to generate wall aspect, wall height, and sky view factor within the UMEP application [36]. In the next step, SOLWEIG merges both datasets, meteorological and preprocessed spatial data output to produce Tmrt and the hourly pattern of shadow in the study area. Then, the SOLWEIG analyzer is the final stage for enabling results to be statistically calculated and plotted based on the SOLWEIG outputs such as the spatial distribution of Tmrt, sunlit, shadow, and more. Vectorizing the results and applying the PET index results in a map displaying the regions in the priority of heat mitigation called hot-spots map, a guide map appropriated for efficient intervention, and vegetation planning, see Figure 7.
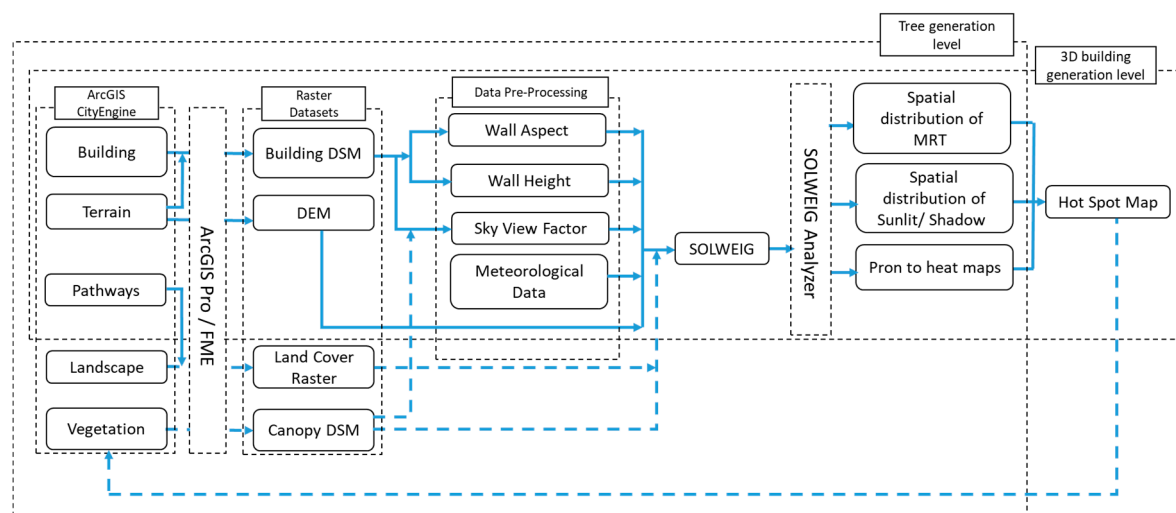
Figure 7. The detailed flowchart of data preparation and processing for hot spot map and vegetation planning.

2.5. Meteorological Data and Climate Scenario

Increasing the population of urban areas leads to a massive need for new development and infrastructure, and cities are preparing their new action plans to face the extensive demand for the future. As discussed, the proposed scenario is a response to a future condition. Hence the research leveraged a predicted climate scenario developed by Hosseini et al. 2020 [41]. The climate scenario for this research is derived from the GFDL_ESM2 model [42] concerning climate change resulting from greenhouse gas emissions. The model data are downscaled to Montréal-Pierre Elliott Trudeau international airport with an hourly resolution provided for the next 30 years, year-by-year, taking into account the pressure of population increase, slow income growth with the modest rates of technology (RCP 8.5 W/m^2 scenario [43]) from 2020 onwards. The model used the statistically-based correction to eliminate the discovered errors comparing the previous forecast with the observed data. Then, through applying a classification method used daily monitored data from 1953 to 2014 and regression techniques, a model was trained to generate hourly weather parameters focusing on temperature, radiation, wind speed, and atmospheric pressure [41]. The temperature variation resulting from climate change is significantly higher than other factors; see Figure 8b,d,f. Based on the analysis of projected years, the intensity and frequency of extreme heat have a strong tendency to increase if no greenhouse gas mitigation plan is premeditated.

Reviewing the weather data analysis led by the RCP8.5 scenario represents the significant temperature change in Montreal. In 2047, this city experiences the warmest period and desperate need for cooling load [41]. That was the key point to pick up 2047 weather data as the input of research for the Tmrt modeling and evaluation. In this year, the average temperature is expected to increase by 2.76 K, as if 5.25 K added to the average of wintertime and 1.54 K added to the average of summer days, see Figure 8b. Comparing important weather profile factors for 2020 and 2047, the period of heat, the average daily temperature more than 30 °C, for 2047 is expected to be extended from one month, July in 2020, to three months starting in May and ending in August. The scenario predicts the count of hours more than 20 °C will increase 6.5%, from 1580 h to 2138 h in 2047, and Montreal needs to be prepared for 153 more hours of air temperature higher than 30 °C. The selected temporal period of Tmrt assessment for the project is two consecutive days from August 10 at 1:00 AM to August 11 at 24:00 in 2047, during which the temperature variation is between a minimum of 20 °C during night time and a maximum 35 °C at 16:00 of the first day. The average temperature of these two days is 26.19 °C, almost 6 K more than the same time in 2020, see Figure 8a. As the input meteorological data for the alternative scenario, the model relies on three components of solar radiation flux during the day time, the global horizontal as the primary factor, direct normal and diffuse horizontal radiation with

the hourly average 348, 811 and 60 Wh.m^{-2}, respectively. By comparing the radiation flux for the same days in 2020 and 2027, the direct and diffuse radiations do not show notable changes and are entirely overlaid in Figure 8e. However, the average of global horizontal radiation has increased significantly by 108 Wh.m^{-2} relatives to reference days in 2020, see in Figure 8c. The average wind speed for the target two days is 2.73 m.s^{-1}, and during which the cloudiness of the sky is at the minimum.
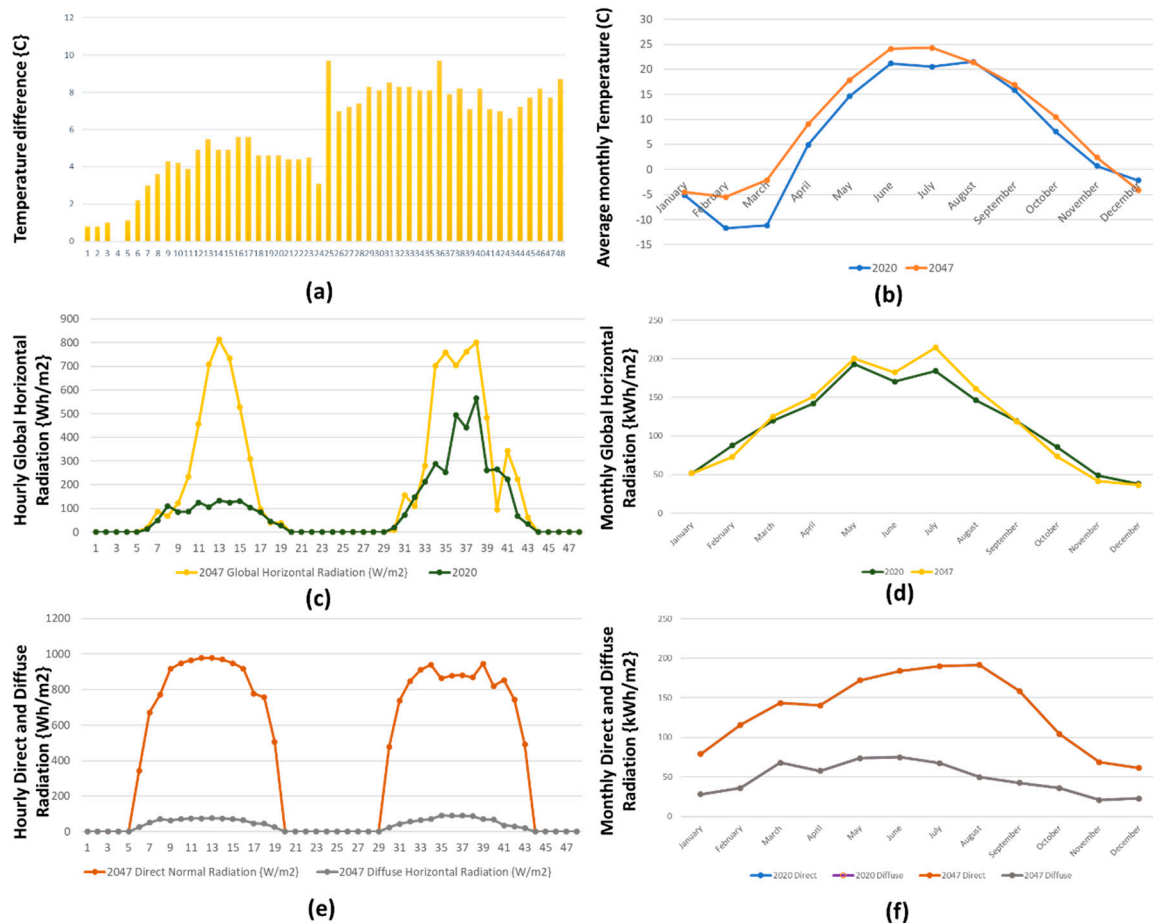

Figure 8. (**a**) The temperature difference between two alternative days of project (10 and 11 of August) in 2047 and 2020; (**b**) pairwise comparison of the average monthly temperature for 2020 and 2047; (**c**) pairwise comparison of hourly global radiation flux for two alternative days of project (10 and 11 of August 2020 and 2047); (**d**) pairwise comparison of monthly global horizontal radiation flux for 2020 and 2047; (**e**) pairwise comparison of hourly direct and diffuse radiation flux for two alternative days of project (10 and 11 of August 2020 and 2047); (**f**) pairwise comparison of monthly direct and diffuse radiation flux for 2020 and 2047.

3. Results and Discussion

3.1. Effect of Wall Surface Albedo Variation on the Mean Daytime Tmrt

In the absence of vegetation, the distribution of Tmrt is dependent on the configuration layout of the building and properties of surface material, precisely albedo value. Evaluating the effect of the various albedo values on the wall surfaces from 0.75 to 0.15 shows a meaningful decrease in the mean daytime Tmrt by 0.5 K per twenty percent albedo reduction as if the maximum of mean daytime Tmrt would decrease by almost 1.70 K. The open spaces showed the minimum reflection in response to the wall surface albedo variation. In contrast, narrow spaces have a maximum reaction by raising the average of Tmrt by 1 K per 20 percent increase in albedo value, see Table 2. Using albedo in the low value provides more comfortable Tmrt during summer days. However, it may result in uncomfortable

and cold stress in the narrow spaces between buildings, see Figure 9. When changing the wall surface albedo, the ground albedo was assumed the default set (0.20) on the model. The variation of ground surface albedo could be managed either by changing the default value or using the land cover layer produced in raster format. The probability of overestimating the Tmrt due to using the land cover layer discussed by Gála and Kántor (2020) [40] convinced us to use the default value in the rest of the modeling process.

Table 2. The average daytime Tmrt (°C) in different urban spaces when the wall surface albedo changes.

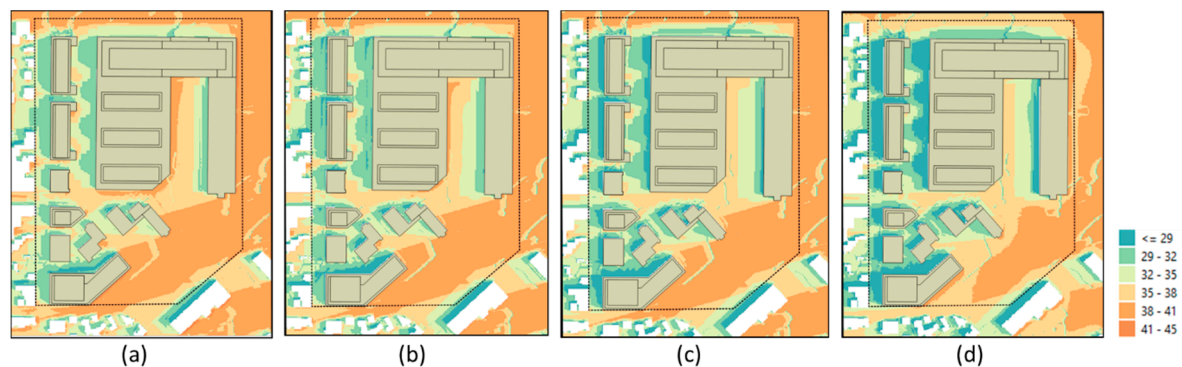| Albedo Value	USp_1	USp_2	USp_3	USp_4	USp_5	USp_Medium	Avg. of the Site	Min–Max of the Site
Avg. SVF	0.7	0.56	0.56	0.72	0.97	0.45 >		
0.75	35.81	32.38	32.96	37.47	40.00	31.72	37.43	27.24–45.38
0.55	35.09	31.48	32.05	36.80	39.88	30.82	36.94	26.50–43.53
0.35	34.37	30.58	31.15	36.13	39.76	29.73	36.45	25.73–41.66
0.15	33.64	29.68	30.24	35.43	39.64	28.75	35.95	24.80–40.30
Avg. of Tmrt Differences	0.72	0.90	0.90	0.68	0.12	1.00	0.50	0.82–1.69

Figure 9. Spatial distribution of mean daytime Tmrt using different wall surface albedo from high to low value: (**a**) albedo = 0.75; (**b**) albedo = 0.55; (**c**) albedo = 0.35; (**d**) albedo = 0.15.3.2. The Spatiotemporal Distribution of Tmrt and Identification of Hot-Spots.

By changing the albedo values from 0.35 to 0.75, the results of SOLWEIG for the hourly Tmrt on the spots distributed in the site showed a considerable temperature variation at the peak hour, almost 5 K for the points near the buildings and less than 3 K for the central points in the surrounded urban spaces. Based on the literature review, the results are prone to overestimation for the points near the buildings [24]. Moreover, it was expected to see the maximum variation of Tmrt after or before the peak hour while the model starts dropping right after the peak to disappear by sundown [25]. Since the model is not comparable with the observed data, it suggested more investigation of the model's accuracy concerning the effect of the material's albedo for the next research. However, the default value of wall surface albedo, 0.20, has been tested and verified in many relevant studies using the SOLWEIG model [11,14,37–40]. Thus, we used it in the research since it is near the albedo of selected materials for buildings in the study area.

The measured correlation, R2 (the coefficient of determination), between the albedo value and the average daytime Tmrt is 0.23. It is not significant compared to the sky view factor effect, which provides a strong positive correlation with the value of R2 equal to 0.92. It states the high sky view factor goes with high Tmrt and determines where the tendency of the area to heat stress increases, and on the other side, in which level of sky exposure, spaces have the primary condition for heat relief Figure 10. The spatial distribution of mean daytime Tmrt classified based on physiological equivalent temperature (PET) demonstrates the thermal comfortability of urban spaces resulted from variation of sky view factor and solar access, see Figure 10b. PET index relies on dry temperature, relative humidity, wind speed,

and mean radiant temperature to represent the levels of thermal perception and physiological stress; see in Table 3 [44].
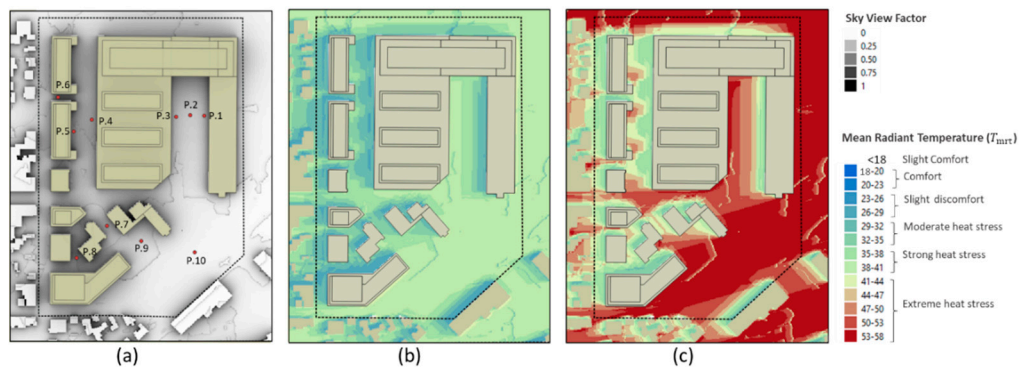

Figure 10. (**a**) The distribution of the sky view factor resulted from the building design and the spread of focal spots all over the site; (**b**) the distribution of mean daytime Tmrt classified by PET index; (**c**) the distribution of mean Tmrt classified by PET index through the hottest period of the days (12:00–19:00).

Table 3. Thermal sensitivity and grads of physiological stress, according to Mayer and Matzaraki [44].

PET (°C) Range	Above +41	+35 to +41	+29 to +35	+29 to +23	+23 to +18	+18 to +13	+13 to +8	+8 to +4	Below 4
Heat stress category	Extreme heat stress	Strong heat stress	Moderate heat stress	Slight discomfort	Comfort	Slight comfort	Moderate cold stress	Strong cold stress	extreme cold stress

Increasing 25% of the average sky view factor give rise almost 3.5 K to the mean daytime Tmrt of the urban spaces, although the direction of urban spaces has a considerable effect in the project's case. The spatial pattern of mean daytime Tmrt in Figure 10b demonstrates the general increase in Tmrt at a distance from west-facing walls to the east-facing walls and north-facing walls to the south-facing walls in the N–S and the E–W canyons, respectively. The pattern and duration of shadow and sunlit area change the mean daytime Tmrt over a short distance in the surrounded urban spaces up to 25 K. When air temperature and global and direct radiation are at a high level, 12:00 to 19:00, the average of Tmrt exceeds the extreme heat stress, 41 °C, see Figure 8c. During this period, 75% of the site is sunlit, see Figure 11 and demands the dire need for heat mitigation. However, some areas are in buildings' shade and provide a moderate comfort level. The spatiotemporal behavior of Tmrt is different in each urban space, depending on the characters and direction of the surrounding buildings.
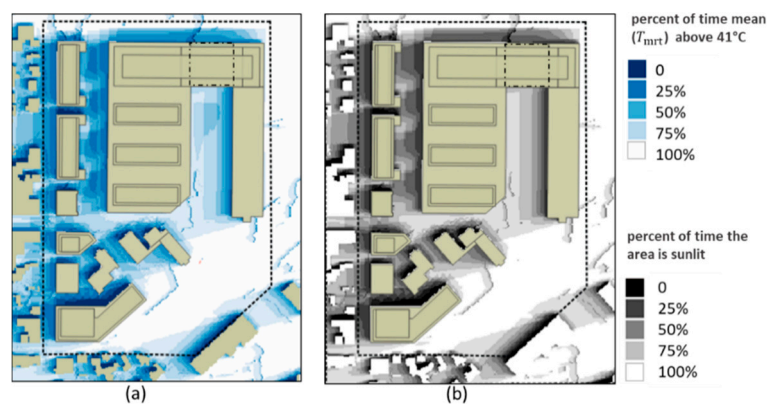

Figure 11. (**a**) The percent of the time that the mean daytime Tmrt is above 41 °C during the hottest period of days (12:00–19:00); (**b**) the percent of the time which the area covered sunlit during the hottest period of days (12:00–19:00).

In the public square of USp_1, the N_S wide canyon, the differences between East and West of the site start around noon. It takes one hour for the west and center of the site to reach the peak of Tmrt at 63 °C, while it takes 5 h for the east side with almost 10 K reduction in the peak level. During the five hours, the discrepancy of temperature overtakes 25 K over the public square's eastern and western sides. The most extended duration of heat stress is for the western two-thirds of the site, with 7 h of extreme heat stress. In contrast, the eastern part of the site undergoes less than two hours above 41 °C, see Figure 12a. It is worthy of indicating in the N_S squares that the eastern building's effect is more than western in providing efficient shadow during the hottest period of the day. The next canyons, USp_2 and USp_3, directed in N_S, are influenced by a super building located on the eastern side of urban spaces. The buildings have a complex form above 10 m from the street line. At this level, the buildings have a 5 m setback and are converted to a detached form with almost 23 m distance between them, see Figure 2. For the non-uniform geometry modeling, the evaluation of aspect ratio could not be beneficial, and measuring the sky view factor in different sections of space is more reliable. The design effect resulted in the wavy sky view factor, and consequently, the curvy distribution of mean daytime Tmrt across the canyon changes between 12 K to 28 K for less than 2 h. There is a significant delay for spaces to reach their peak because of the surrounding buildings' elevation, see Figure 12b. It happens after 15:00 for the western side and at 18:00 for the eastern side of the spaces. Overall, the east side of the urban spaces is shaded 70% of the daytime and represents an area with slight discomfort. On the other side, the west side is located in moderate heat stress for 85% of the time, see Figure 11. The duration of heat stress above 41 °C is less than 4 h, only for 30% of the site near the east-facing walls.
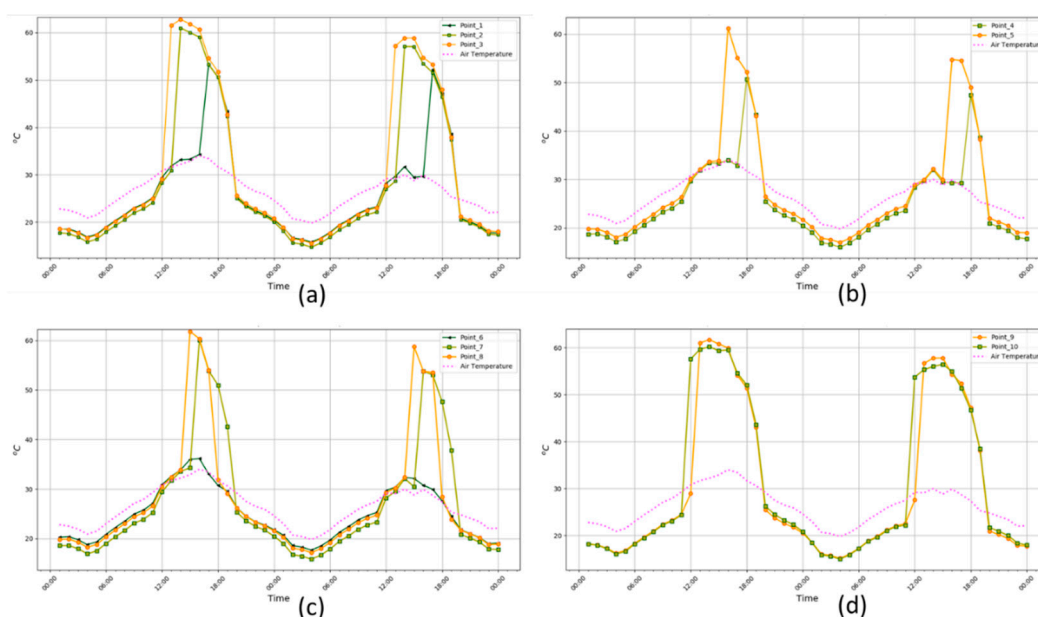

Figure 12. The temporal and spatial distribution of hourly Tmrt for focal spots in the urban spaces demonstrated in Figure 10a; (**a**) points (1,2,3); (**b**) points (4,5); (**c**) points (6,7,8); (**d**) points (9,10).

The courtyard and public park, USp_4, and USp_5, have almost the same behavior in their central area due to the wide aspect ratio, see Figure 12d. However, the effect of surrounded wall surfaces increases the amount of longwave radiation received for the courtyard. This results in 2 K growth of Tmrt at the peak hour compared to the public park and has also reduced the time in which space is illuminated by 28%. In the absence of surrounding buildings, the heating up of the public park starts earlier than the other regions, and the duration of heat stress goes above 7 h. The last group of spaces connecting the principal urban spaces and buildings with the average sky view factor lower than 0.45 is notably affected by surrounding walls. In these spaces, the building walls decrease their shortwave

radiation access during the day time. It provides nearly 76% of the time under shade during the heat stress period. For this group of urban spaces, the average daytime Tmrt is 36 °C, almost 11 K lower than the average of the site, see Figure 12c.

To achieve thermal comfort at efficient and context-sensitive tree placement as the principal strategy, we overlaid the spatial map of mean Tmrt during heat stress with the designed human traffic pathway. Applying the extreme heat threshold above 41 °C based on the PET index, it is possible to cluster the regions distributed under extreme stress, see Figure 13a. The clustered map demonstrates the preference area for heat mitigation practice in the study area's dense structure. The footpath, located in the public park and far from surrounded walls, receives a high solar radiation level with mean Tmrt over 57 °C. There is almost the same heat stress for pathways located around the east-facing walls in the urban spaces USp_1, USp_2, USp_3, and USp_4, providing the average Tmrt of 52, 42, 41, 57 during the hottest period of the day, respectively. In the second level, heat mitigation action goes for the series of pathways distributed in the rest of the site connecting buildings and principle urban spaces, medium spaces with the average sky view factor more than 0.45. The variation of the sky view factor and shading pattern results in noncontinuous regions above 41 °C. These areas solicit for deliberate action and pointwise heat mitigation strategy. The pathway area located in the proximity of the west-facing walls and spaces with the lower sky view factors (0.45>) is in the shade of the surrounded walls for 74% of the time and displays a nonsignificant demand for thermal comfort by providing the mean Tmrt of 36 °C during the heat stress time, see Figure 11.
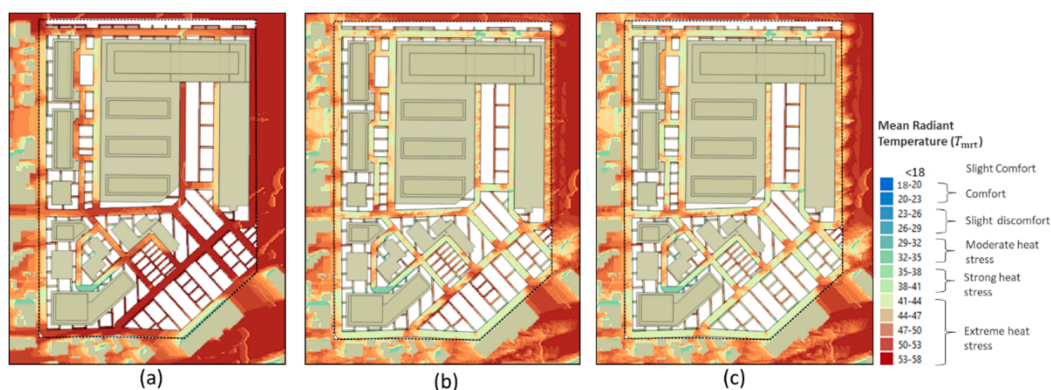

Figure 13. The overlaid map of the alternative pathway and the mean Tmrt for the hottest period of days (12:00–19:00) with the classification of PET in three conditions; (**a**) the baseline map without tree planting scenario; (**b**) the first level of tree placement with the priority of pathways; (**c**) the second level of tree placement with the priority of some urban spaces.

3.2. Heat Mitigation through Tree Plantation

To systematically place the trees in the first action, the clustered pathway above 41 °C in the TIF format got vectorized through QGIS before transferring to CityEngine. Inside CityEngine, using the complete street rule CGA code from D.Wasserman, Norway maple trees are placed on the pathway sidewalks, which falls on the central axis of the clustered pathways. The trees' placing was conscious with 10 m distancing regarding the average canopy cover for the target Norway maple (10 m-diameter) with 15 m height. The tree generation process's outcome leads to 264 trees with a sufficient canopy coverage density of 19% of the site (30% of the landscape) as the mitigation action strategy. The outcome of tree planting results in almost 8.5 K improvement of mean Tmrt within pathways and 7.5 K all over the site compared to without tree condition during the stress time, see Figure 13b. Figure 14a shows the improvement of average Tmrt during the hottest period of the day, and Figure 14b represents the differences between the conditions, with and without tree placement. The tree placement in pathways also upgrades the average of Tmrt in urban spaces by 5 K, demonstrated in Table 4. This process purposely was focused on the pathways as the first level of thermal comfort betterment and applied

the isolated-linear strategy of tree planting. However, the clustered strategy of tree placement is more recommended for a more substantial effect [19].
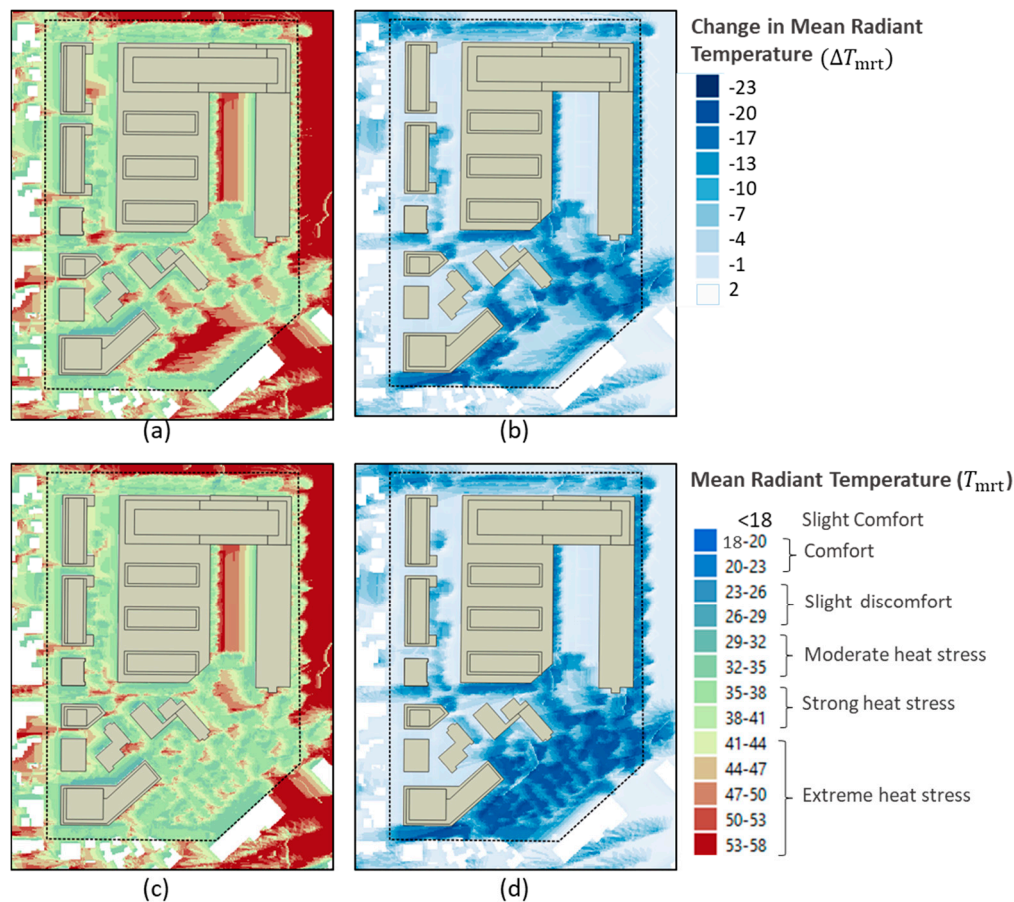

Figure 14. Average Tmrt for the hottest period of days (12:00–19:00) following the strategic addition of trees in level 1 (**a**) and level 2 (**b**); the change (Δ) in Tmrt with the baseline map (the condition without tree placement) in level 1 (**b**) and level 2 (**d**).

In terms of improving thermal comfort in urban spaces, depending on their timing use and level of activity, it is required to repeat the process of overlaying of the mean Tmrt during the heat stress with the target urban space boundaries and applying the threshold of above 41 °C for the area under extreme stress. Subtracting the region out of stress provides a clustered map for the second level of heat mitigation practice through tree placement. Like the first level, the second level's clustered map output is converted to shapefile using QGIS and imported to CityEngine. Within CityEngine, for all the polygon patches of open spaces falling on the heat stress region, the CityEngine inbuilt "plant loader.cga" rule file is tweaked and applied to the open space polygon patches to match the boundary condition of 1 tree per 120 square meters.

The second level of tree generation results in increasing the average density of trees in the site by 4% of the site (6% of the landscape), 58 trees. It leads to the general improvement of mean Tmrt by 1.3 K in the site meantime 1 K in the pathways compared to the first mitigating plan during the hottest period of the day, see Figure 13c. Moreover, the mean Tmrt changes 3.5 K to better for three target spaces of USp_2, USp_4, and USp_5, which were subject to new improvement because of their local activity purposes and public park functionality, see Table 4. Figure 14c depicts the improvement of mean Tmrt in the site, and Figure 14d represents the difference of Tmrt between the condition without tree and the summation of the first and second level of tree placement.

Table 4. The average of mean daytime Tmrt in different urban spaces where vegetation strategy is applied during the hottest period of day (12:00–19:00).

Main Parameters	USp_1	USp_2	USp_3	USp_4	USp_5	USp_Medium	Avg. of the Site	Min–Max of the Site
Avg. SVF	0.7	0.56	0.56	0.72	0.97	0.45 >		
Average of Tmrt L1	40.51	46.17	39.60	49.73	53.97	36.90	47.02	30.34–56.98
Average of Tmrt L2	36.18	42.76	39.23	39.34	42.83	36.42	39.80	30.34–56.98
Average of Tmrt L3	36.18	42.76	37.76	36.81	36.88	36.42	38.52	30.34–54.04
Percent of time above 41 °C (baseline)	45	67	42	78	95	24	67	0–100
Percent of time above 41 °C in level 1	19	50	42	29	52	24	35	0–100
Percent of time above 41 °C in level 2	19	50	33	17	17	24	29	0–100

4. Conclusions

This research identifies a systematic workflow to evaluate and upgrade the outdoor thermal comfort relying on the contribution of 3D city modeling and climate assessment application for various time scales. A case study district under development in Montreal was used to analyze 3D geometry's impact on thermal comfort. Geometries were generated using the ArcGIS CityEngine. The generated spatial design was rasterized to serve the SOLWEIG program to model the spatiotemporal distribution of mean radiant temperature (Tmrt) as an outdoor thermal comfort indicator. Analyzing the outcome of SOLWEIG reveals the duration and pattern of the area under heat stress. The spatial variation of Tmrt demonstrates almost 25 K difference over the spaces investigated. One of the critical reasons was the variation of the average sky view factor resulting from surrounding buildings, with a non-uniform distribution of geometry in three dimensions. Moreover, the North-South dominant direction for some urban spaces resulted in a durable shadow for the area adjacent to the west-facing walls. Whereas the areas in the proximity of east-facing walls in the wide canyons suffered from being long-time exposed to solar irradiance during the hottest period of the day. Moreover, varying the albedo value on the wall surfaces showed an almost 0.5 K decrease per twenty percent reduction of albedo. Focusing on the albedo value, deep canyons with low sun accessibility showed more sensitivity to albedo effects, and their average mean daytime Tmrt changes more than wider canyons.

Analyzing and classifying the results with the physiological equivalent temperature (PET) index indicated the potential regions under extreme heat stress. By overlaying the classified map and the human walkway's principal structure, the priority of regions subject to heat mitigation action were clustered as a hot-spots map. The hot-spots map converted to polygon shapefile was used for automated tree generation in the CityEngine and converted to vegetation DSM for reassessment in the SOLWEIG program. The workflow was iterated two times. In the first round, the heat mitigation action's target area was the improvement of human walkways. The response strategy results in proposing 264 number of trees with a 19% density of canopy coverage over the site (30% of the landscape). It led to improving the mean Tmrt during the hottest period of the day by 7.5 K in the entire study area, 8.5 K on the footpaths, and 5 K in the urban spaces. In the second try, the focus was on the urban space enhancement regarding their level of activity. In this case, the local community spaces and the park were in priority. The second intervention's outcome added 58 more trees and increased tree canopy density by 4% (6% of the landscape). At this level, the mean Tmrt of the site was reduced by 1.3 K and determined urban spaces by 3.5 K during the hottest period of the day.

The designed workflow is scalable and allows for the outdoor thermal evaluation in multiple urban levels. The simultaneous designing, visualizing, and assessment supports architects and urban designers for a collaborative practice toward climate-responsive decision-making to reduce the cost of human errors, as today's design decision has implications for the next decades. However, using such a workflow, as demonstrated in the present work, reiterates the need for urban designers, geoinformatics, and sustainability experts to work hand-in-hand. That is because executing such a 3D city modeling

driven workflows needs an acceptable level of experience and familiarity with the geographic information system (GIS), 3D data modeling methods, and basic computer programing ability in the case of using ArcGIS CityEngine. From the technical side in the SOLWEIG model, the hourly Tmrt on the spots near the buildings, in a nonuniformed surrounding, is prone to overestimating around the peak hour when the albedo value increases significantly from 0.15 to 0.75. Whereas in the central points with uniform surroundings and lower albedo value, the estimation of hourly Tmrt is close to the expected influence of albedo effect, namely lower than 2 K.

The next issue is relevant to converting 3D building geometry with open space between the bottom surface of a bridge-type building and the ground surface (Figure 6) provided complication and unreal data when converting to DSM. This problem resulted in missing correct data under the bridge building section and, consequently, no tree plantation suggestion could be made through the workflow. Such an issue can result in a wrong heat stress calculation from models such as SOLWEIG for which primary inputs are raster datasets. Since such complexity in the arrangement of building blocks is also available in the real-world, development of SOLWEIG type models which can directly accept 3D city models as inputs are suggested. It reduces the information loss, which happens while converting 3D city model geometries to raster datasets. Finally, this study clearly demonstrates the workflow's capacity to provide an effective collaboration between 3D city modeling and climate assessment application to mitigate outdoor thermal stress through objective and systematic intervention (tree placement), which is currently a challenge for urban planners due to the lack of easy-to-use tools.

References

1. Canada's Changing Climate Report. Available online: https://changingclimate.ca/CCCR2019/ (accessed on 23 September 2020).
2. Bastin, J.-F.; Clark, E.; Elliott, T.; Hart, S.; Hoogen, J.V.D.; Hordijk, I.; Ma, H.; Majumder, S.; Manoli, G.; Maschler, J.; et al. Correction: Understanding climate change from a global analysis of city analogues. *PLoS ONE* **2019**, *14*, e0224120. [CrossRef] [PubMed]
3. Communicating the Health Risks of Extreme Heat Events—Canada.ca. Available online: https://www.canada.ca/en/health-canada/services/environmental-workplace-health/reports-publications/climate-change-health/communicating-health-risks-extreme-heat-events-toolkit-public-health-emergency-management-officials-health-canada-2011.html (accessed on 24 September 2020).
4. Quebec Says Up to 70 People May Have Died in Connection with Recent Heat Wave | CTV News. (n.d.). published on 9 July 2018. Available online: https://www.ctvnews.ca/canada/quebec-says-up-to-70-people-may-have-died-in-connection-with-recent-heat-wave-1.4006431 (accessed on 17 November 2020).
5. Canada Health Act Annual Report 2011–2012—Canada.ca. Available online: https://www.canada.ca/en/health-canada/services/health-care-system/reports-publications/canada-health-act-annual-reports/report-2011-12.html (accessed on 24 September 2020).
6. Environment and Climate Change Canada—Weather and Meteorology—Weather and Meteorology—Glossary. Available online: https://www.ec.gc.ca/meteo-weather/default.asp?lang=En&n=B8CD636F-1&def=allShow (accessed on 24 September 2020).
7. Mayer, H.; Hoppe, P. Thermal comfort of man in different urban environments. *Theor. Appl. Climatol.* **1987**, *38*, 43–49. [CrossRef]
8. Thorsson, S.; Rocklöv, J.; Konarska, J.; Lindberg, F.; Holmer, B.; Dousset, B.; Rayner, D. Mean radiant temperature—A predictor of heat related mortality. *Urban Clim.* **2014**, *10*, 332–345. [CrossRef]

9.   ASHRAE Handbook Online. Available online: https://www.ashrae.org/technical-resources/ashrae-handbook/ashrae-handbook-online (accessed on 23 September 2020).

10.   Nazarian, N.; Fan, J.; Sin, T.; Norford, L.; Kleissl, J. Predicting outdoor thermal comfort in urban environments: A 3D numerical model for standard effective temperature. *Urban Clim.* **2017**, *20*, 251–267. [CrossRef]

11.   Lindberg, F.; Grimmond, C.S.B. The influence of vegetation and building morphology on shadow patterns and mean radiant temperatures in urban areas: Model development and evaluation. *Theor. Appl. Climatol.* **2011**, *105*, 311–323. [CrossRef]

12.   Thorsson, S.; Lindberg, F.; Björklund, J.; Holmer, B.; Rayner, D. Potential changes in outdoor thermal comfort conditions in Gothenburg, Sweden due to climate change: The influence of urban geometry. *Int. J. Climatol.* **2011**, *31*, 324–335. [CrossRef]

13.   Ali-Toudert, F.; Mayer, H. Numerical study on the effects of aspect ratio and orientation of an urban street canyon on outdoor thermal comfort in hot and dry climate. *Build. Environ.* **2006**, *41*, 94–108. [CrossRef]

14.   Lindberg, F.; Holmer, B.; Thorsson, S.; Rayner, D. Characteristics of the mean radiant temperature in high latitude cities—Implications for sensitive climate planning applications. *Int. J. Biometeorol.* **2014**, *58*, 613–627. [CrossRef]

15.   Thom, J.K.; Coutts, A.; Broadbent, A.M.; Tapper, N.J. The influence of increasing tree cover on mean radiant temperature across a mixed development suburb in Adelaide, Australia. *Urban For. Urban Green.* **2016**, *20*, 233–242. [CrossRef]

16.   Lindberg, F.; Thorsson, S.; Rayner, D.; Lau, K. The impact of urban planning strategies on heat stress in a climate-change perspective. *Sustain. Cities Soc.* **2016**, *25*, 1–12. [CrossRef]

17.   Johansson, E. Influence of urban geometry on outdoor thermal comfort in a hot dry climate: A study in Fez, Morocco. *Build. Environ.* **2006**, *41*, 1326–1338. [CrossRef]

18.   Oke, T.R.; Johnson, G.T.; Steyn, D.G.; Watson, I.D. Simulation of surface urban heat islands under "ideal" conditions at night part 2: Diagnosis of causation. *Boundary-Layer Meteorol.* **1991**, *56*, 339–358. [CrossRef]

19.   Wang, Y.; Akbari, H. The effects of street tree planting on Urban Heat Island mitigation in Montreal. *Sustain. Cities Soc.* **2016**, *27*, 122–128. [CrossRef]

20.   Konopacki, S.; Akbari, H.; Gartland, L. *Cooling Energy Savings Potential of Light-Colored Roofs for Residential and Commercial Buildings in 11 US Metropolitan Areas*; Berkeley National Laboratory: Berkeley, CA, USA, 1997. [CrossRef]

21.   Akbari, H.; Pomerantz, M.; Taha, H. Cool surfaces and shade trees to reduce energy use and improve air quality in urban areas. *Sol. Energy* **2001**, *70*, 295–310. [CrossRef]

22.   Çengel, Y.A. *Heat & Mass Transfer: Fundamentals and Applications*; Tata McGraw-Hill: NewDelhi, India, 2011.

23.   Erell, E.; Pearlmutter, D.; Boneh, D.; Bar Kutiel, P. Effect of high-albedo materials on pedestrian heat stress in urban street canyons. *Urban Clim.* **2014**, *10*, 367–386. [CrossRef]

24.   Alchapar, N.L.; Correa, E. Comparison of the performance of different facade materials for reducing building cooling needs. In *Eco-Efficient Materials for Mitigating Building Cooling Needs*; Woodhead Publishing: Cambridge, UK, 2015; pp. 155–194. [CrossRef]

25.   Li, H. *Pavement Materials for Heat Island Mitigation: Design and Management Strategies*; Elsevier: Amsterdam, The Netherlands, 2015.

26.   Montreal climate: Average Temperature, Weather by Month, Montreal Weather Averages—Climate-Data.org. Available online: https://en.climate-data.org/north-america/canada/quebec/montreal-3704/ (accessed on 23 September 2020).

27.   Padsala, R.; Coors, V. Conceptualizing, managing and developing: A web-based 3D city information model for urban energy demand simulation. In Proceedings of the UDMV15: Eurographics Workshop on Urban Data Modelling and Visualisation, Delft, The Netherlands, 23 November 2015; pp. 37–42. [CrossRef]

28.   Watson, B.; Müller, P.; Veryovka, O.; Fuller, A.; Wonka, P.; Sexton, C. Procedural urban modeling in practice. *IEEE Comput. Graph. Appl.* **2008**, *28*, 18–26. [CrossRef]

29.   Padsala, R.; Fink, T.; Peters-Anders, J.; Gebetsroither-Geringer, E.; Coors, V. From Urban Design to Energy Simulation—A Data Conversion Process Bridging the Gap Between Two Domains. In Proceedings of the 25th International Conference on Urban Planning, Regional Development and Information Society, Aachen, Germany, 15–18 September 2020; Volume 8, pp. 365–375.

30.   Grêt-Regamey, A.; Celio, E.; Klein, T.M.; Hayek, U.W. Understanding ecosystem services trade-offs with interactive procedural modeling for sustainable urban planning. *Landsc. Urban Plan.* **2013**, *109*, 107–116. [CrossRef]

31. Biljecki, F.; LeDoux, H.; Stoter, J. Generation of multi-LOD 3D city models in CityGML with the procedural modelling engine Random3Dcity. In Proceedings of the ISPRS Annals of the Photogrammetry, Remote Sensing and Spatial Information Sciences, Delft, The Netherlands, 5 September 2016. [CrossRef]

32. Fink, T.; Koenig, R. Integrated parametric urban design in grasshopper/rhinoceros 3D demonstrated on a master plan in Vienna. In Proceedings of the 37 eCAADe and XXIII SIGraDi Joint Conference, "Architecture in the Age of the 4th Industrial Revolution", Porto, Portugal, 11–13 September 2019; pp. 313–322. [CrossRef]

33. Reitz, T.; Schubiger-Banz, S. The ESRI 3D city information model. In *IOP Conference Series: Earth and Environmental Science*; IOP Publishing: Bristol, UK, 2014; Volume 18, p. 12172. [CrossRef]

34. Modèle Numérique de Terrain—Modèle Numérique de Terrain (MNT) 2015—Arrondissement Lachine—CityGML—PortailDonnéesOuvertes. Available online: http://donnees.ville.montreal.qc.ca/dataset/modele-numerique-de-terrain-mnt/resource/54cb894b-551d-47ba-9cd5-0caf2a200ab1 (accessed on 23 September 2020).

35. GitHub—D-Wasserman/Complete_Street_Rule: The Complete Street Rule for ArcGIS CityEngine is a Scenario-Oriented Design Tool Intended to Enable Users to Quickly Create Procedural Generated Multimodal Streets. Available online: https://github.com/d-wasserman/Complete_Street_Rule (accessed on 23 September 2020).

36. UMEP Manual—UMEP Manual Documentation. Available online: https://umep-docs.readthedocs.io/en/latest/index.html (accessed on 17 November 2020).

37. Lindberg, F.; Holmer, B.; Thorsson, S. SOLWEIG 1.0—Modelling spatial variations of 3D radiant fluxes and mean radiant temperature in complex urban settings. *Int. J. Biometeorol.* **2008**, *52*, 697–713. [CrossRef]

38. Lindberg, F.; Onomura, S.; Grimmond, C.S.B. Influence of ground surface characteristics on the mean radiant temperature in urban areas. *Int. J. Biometeorol.* **2016**, *60*, 1439–1452. [CrossRef]

39. Konarska, J.; Lindberg, F.; Larsson, A.; Thorsson, S.; Holmer, B. Transmissivity of solar radiation through crowns of single urban trees—Application for outdoor thermal comfort modelling. *Theor. Appl. Climatol.* **2014**, *117*, 363–376. [CrossRef]

40. Gál, C.V.; Kántor, N. Modeling mean radiant temperature in outdoor spaces, A comparative numerical simulation and validation study. *Urban Clim.* **2020**, *32*, 100571. [CrossRef]

41. Hosseini, M.; Bigtashi, A.; Lee, B. Generating future weather files under climate change scenarios to support building energy simulation—A machine learning approach. *Energy Build.* **2020**, *184*, 110543. [CrossRef]

42. Dunne, J.P.; John, J.G.; Shevliakova, E.; Stouffer, R.J.; Krasting, J.P.; Malyshev, S.L.; Milly, P.C.D.; Sentman, L.T.; Adcroft, A.J.; Cooke, W.; et al. GFDL's ESM2 global coupled climate–Carbon Earth system models. *Part II: Carbon System Formulation and Baseline Simulation Characteristics. J. Clim.* **2013**, *26*, 2247–2267.

43. Riahi, K.; Rao, S.; Krey, V.; Cho, C.; Chirkov, V.; Fischer, G.; Kindermann, G.; Nakicenovic, N.; Rafaj, P. RCP 8.5—A scenario of comparatively high greenhouse gas emissions. *Clim. Chang.* **2011**, *109*, 33–57. [CrossRef]

44. Matzarakis, A.; Mayer, H.; Iziomon, M.G. Applications of a universal thermal index: Physiological equivalent temperature. *Int. J. Biometeorol.* **1999**, *43*, 76–84. [CrossRef]